

A photometric study of the ages and metallicities of early-type galaxies in A 2218

Ian Smail,¹* Harald Kuntschner,¹ T. Kodama,¹ G. P. Smith,¹ C. Packham,²†
A. S. Fruchter³ and R. N. Hook⁴

¹*Department of Physics, University of Durham, South Road, Durham DH1 3LE*

²*Isaac Newton Group, Apartado 321, 38780 Santa Cruz de La Palma, Tenerife, Canary Islands, Spain*

³*Space Telescope Science Institute, 3700 San Martin Drive, Baltimore, MD21210, USA*

⁴*Space Telescope – European Coordinating Facility, European Southern Observatory, Karl-Schwarzschild-Str. 2, D-85748 Garching bei München, Germany*

Accepted 2000 December 1. Received 2000 November 16; in original form 2000 August 14

ABSTRACT

We present deep optical and near-infrared imaging of the rich cluster A 2218 at $z = 0.17$. Our optical imaging comes from new multicolour *Hubble Space Telescope* WFPC2 observations in the F450W (B_{450}), F606W (V_{606}) and F814W (I_{814}) passbands. These observations are complemented by deep near-infrared, K_s -band imaging from the new INGRID imager on the 4.2-m William Herschel Telescope. This combination provides unique high-precision multicolour optical–infrared photometry and morphological information for a large sample of galaxies in the core of this rich cluster, at a look-back time of ~ 3 Gyr. We analyse the $(B_{450} - I_{814})$, $(V_{606} - I_{814})$ and $(I_{814} - K_s)$ colours of galaxies spanning a range of a factor of 100 in K -band luminosity in this region, and compare them with grids of stellar population models. We find that the locus of the colours of the stellar populations in the luminous ($\geq L_K^*$) early-type galaxies, both ellipticals and S0s, traces a sequence of varying metallicity at a single age. At fainter luminosities ($\leq 0.1L_K^*$), this sequence is extended to lower metallicities by the morphologically classified ellipticals. However, the faintest S0s exhibit very different behaviour, showing a wide range of colours, including a large fraction (30 per cent) with relatively blue colours that appear to have younger luminosity-weighted ages for their stellar populations; 2–5 Gyr. We show that the proportion of these young S0s in the cluster population is consistent with the observed decrease in the S0 population seen in distant clusters, when interpreted within the framework of a two-step spectroscopic and morphological transformation of accreted spiral field galaxies into cluster S0s.

Key words: galaxies: clusters: individual: A 2218 – galaxies: elliptical and lenticular, cD – galaxies: evolution – galaxies: stellar content – infrared: galaxies.

1 INTRODUCTION

Studies using photometric and, more recently, spectroscopic observations of luminous elliptical (E) galaxies in distant clusters have suggested that their luminosity and colour evolution is modest and consistent with passive evolution of stellar populations that are formed at high redshifts, $z > 2-4$ (Aragón-Salamanca et al. 1993; Ellis et al. 1997; Kodama et al. 1998; van Dokkum et al. 1998; Kelson et al. 2000).

The relatively modest evolution seen in the luminous elliptical population in clusters contrasts with the claims of strong evolution in the morphological mix in these environments, specifically the ratio of S0 (lenticular) to elliptical galaxies. Using *Hubble Space Telescope* (*HST*) imaging of 10 clusters at $z > 0.3-0.6$, Dressler et al. (1997) have uncovered a rapid increase in the ratio of S0 to elliptical galaxies towards the present day (see also Fasano et al. 2000). Assuming that the elliptical population is static, they interpret this as a strong rise in the S0 population, from 10–20 per cent at $z \sim 0.5$ (6 Gyr ago) to the 60 per cent seen in present-day rich clusters. This apparent evolution applies to the cluster population that is brighter than about $0.1L_K^*$.

By including information from spectroscopic observations of galaxies in 10 clusters, Poggianti et al. (1999) proposed that the

*E-mail: ian.smail@durham.ac.uk

†Present address: Department of Astronomy, University of Florida, Gainesville, FL 32611, USA.

build-up of S0 galaxies identified by Dressler et al. (1997) resulted from the morphological transformation of accreted-field spiral galaxies into lenticulars. They further suggested that the presence of a large population of red, apparently passive, galaxies with late-type morphologies in the clusters, along with absence of blue S0 galaxies, indicated that the morphological transformation occurs on a longer time scale than the decline in the star formation rates of the accreted-field galaxies (see also Kodama & Smail 2001). Thus they proposed that the galaxies first suffered a decline in their star formation (probably resulting from stripping of their gas reservoirs as they encounter the dense intracluster medium within the cluster potential) and only then had their morphological appearance transformed (perhaps by a completely separate process, e.g. Moore, Lake & Katz 1998).

Nevertheless, if the morphological transformation occurs on a time scale of $\approx 2\text{--}3$ Gyr after the galaxy's entry into the cluster, it may still be possible to identify subtle signatures of this previous activity in the S0 population. Direct comparisons of the estimated stellar population ages for the S0 and elliptical populations can be particularly powerful in this respect. When comparing the composite spectra of the S0 and elliptical populations in three clusters at $z = 0.3$, Jones, Smail & Couch (2000) found no significant differences in the inferred luminosity-weighted ages of the stellar populations in the two classes at a median luminosity of $0.6L_V^*$, and concluded that this supported the two-step transformation model discussed above. A similar degree of homogeneity between the cluster E and S0 galaxies was reported by Ellis et al. (1997) from their study of the rest-frame ($U - V$) colours of early-type galaxies in three clusters at $z \sim 0.5$, although again the strongest constraints were on the more luminous galaxies, $\geq 0.2L_V^*$. However, a more detailed spectral-line analysis of individual lenticular and ellipticals in Fornax (Kuntschner 2000) has suggested that, in this cluster at least, the low-luminosity lenticulars ($\approx 0.1L_V^*$) exhibit typically younger luminosity-weighted ages for their stellar populations than the ellipticals (see also Jørgensen 1999).

Work on the relative ages of cluster ellipticals and lenticulars continues using new combinations of spectral line indices to break the degeneracy between age and metallicity (Worthey 1994; Vazdekis & Arimoto 1999; Kuntschner 2000). At higher redshift such studies can be observationally expensive, requiring relatively large amounts of 4- and 8-m time, as well as efficient multi-object spectrographs (Kelson et al. 1997; Jørgensen et al. 1999; Ziegler et al. 2001). However, recent developments in stellar population modelling (e.g. Vazdekis et al. 1997; Kodama & Arimoto 1997; Bruzual & Charlot 2000) have suggested that it may be possible to break the age-metallicity degeneracy using observationally cheaper photometric analysis, if it includes both optical and near-infrared (H or K) photometry (an idea originally proposed by Aaronson 1978, see Peletier & Balcells 1996 for an early demonstration). In this paper we explore this possibility using new, high-quality observations of the galaxy population in the core of the rich cluster A 2218 ($z = 0.17$) from *HST* and the new INGRID near-infrared imager on the William Herschel Telescope (WHT). We derive precise optical and optical-infrared colours and morphologies for a large sample of galaxies across a 6-mag range in near-infrared luminosity down to $K_s = 19$ ($0.02L_K^*$) in this field and compare them to the predictions of the latest stellar evolutionary models. We also compare the constraints we derive for individual galaxies with the recent spectroscopic study of A 2218 by Ziegler et al. (2001). We discuss our observations and their reduction in the next section, our results in Section 3 and

present our conclusions in Section 4. Throughout we assume $q_0 = 0.5$ and $h = 0.5$ in units of $100 \text{ km s}^{-1} \text{ Mpc}^{-1}$. In this cosmology, the look-back time to A 2218 is 3 Gyr, the angular scale at the cluster is $1 \text{ arcsec} \equiv 4.3 \text{ kpc}$ and $K_s^* = 14.7$ (adopting $M_K^* = -25.1$, Cole et al. 2001).

2 OBSERVATIONS, REDUCTION AND ANALYSIS

2.1 *HST* optical imaging

The *HST* imaging analysed here was obtained as part of the Early Release Observations (ERO) from WFPC2 after the SM-3a servicing mission in 2000 January. The observations comprise six orbits in both F450W and F814W passbands and five orbits in F606W, giving total integration times of 12.0, 10.0 and 12.0 ks respectively. These exposures were each broken into 1000 s sub-exposures which were spatially offset from each other by sub-pixel shifts, to allow drizzle-reconstruction of the frames to recover some of the information lost as a result of the under-sampling of the *HST* point spread function (PSF) by the WFC pixel arrays.

The individual images were processed using the standard WFPC2 data pipeline, and were subsequently combined and cleaned of cosmic ray and other artifacts using DRIZZLE and related software (Fruchter & Hook 1997) as implemented in IRAF/STSDAS. The final WFC images have an effective resolution (FWHM) of 0.17- and 0.05-arcsec sampling, and cover a field of 5.0 square arcmin. We adopt the photometric calibration of Holtzman et al. (1995) as given on the STScI web pages (http://www.stsci.edu/documents/dhb/web/c32_wfpc2dataanal.fm1.html) to calculate magnitudes in the Vega-based $B_{450}/V_{606}/I_{814}$ system. We use an average gain ratio of 1.988 for the three WFC chips, but note that for the colours based on the *HST* photometry the adopted gain ratio cancels out, and for the *HST*-INGRID colours the uncertainty it introduces is much smaller than the calibration error of the ground-based photometry. The 3σ point source sensitivities in the three passbands are then: $B_{450} = 28.8$, $V_{606} = 29.0$ and $I_{814} = 28.1$. At the redshift of A 2218 these filters sample the cluster population in passbands roughly equivalent to rest-frame U , V and R . We show a true-colour representation of the cluster as seen in the *HST* imaging in Fig. 1.

2.2 INGRID near-infrared imaging

Our near-infrared observations come from the new INGRID imager on the 4.2-m WHT (Packham et al., in preparation). These observations were obtained in commissioning time during 2000 March 22–23. INGRID comprises a 1024^2 HAWAII-2 array at the bent-Cassegrain focus of the WHT, providing a 4.13-arcmin field of view with $0.242\text{-arcsec pixel}^{-1}$ sampling.

Our exposures consist of a total of 8.3-ks integration in the K_s filter, obtained under photometric conditions in $\sim 0.6\text{--}0.8\text{-arcsec}$ seeing. An additional 9.1 ks of J -band imaging was also obtained, and we discuss that elsewhere (Smith et al., in preparation).

The K_s frames consist of multiple sets of three individual 20-s exposures which are co-added in hardware. Each of the co-added 60-s exposures is spatially offset on a non-repeating rectangular grid with a 90-arcsec spacing. They were reduced in a standard manner, using a smoothed illumination correction derived from all the K_s frames that were obtained during the night, and then a local sky correction constructed from a running median of nine frames

median magnitude of $R_{702} = 19.7$, with the faintest four galaxies having $R_{702} \sim 21.5$ – 22 . All of the galaxies are therefore very well detected, with the images of the faintest galaxies having an average signal-to-noise ratio (S/N) per pixel of >10 over areas of ≥ 150 WFC pixels. Based on the comparison of independent classifications of galaxy images with comparable S/N from the MORPHS project (Smail et al. 1997), we estimate that 90 per cent of the classifications are accurate to better than one class, where this represents the difference between e.g. an E and an E/S0. To further test the reliability of our ability to distinguish S0 and ellipticals, we look at the distribution of ellipticities for the two populations (see Ellis et al. 1997). We find that the ellipticity distributions of the two populations are markedly different; a Kolmogorov–Smirnov test gives a probability of only 0.01 per cent that they are drawn from the same parent population, with the S0 ellipticities showing the flatter distribution characteristic of a disc-like morphology. This degree of segregation is similar to that found by Ellis et al. (1997), hence we conclude that the differentiation between S0 and ellipticals in the present work is no worse than that achieved in the MORPHS project.

However, we note that there is considerable debate over the reliability of visual classification of early-type galaxies of the type employed here (compare Dressler et al. 1997; Andreon 1998 and Fabricant, Franx & van Dokkum 2000). Nevertheless, we have

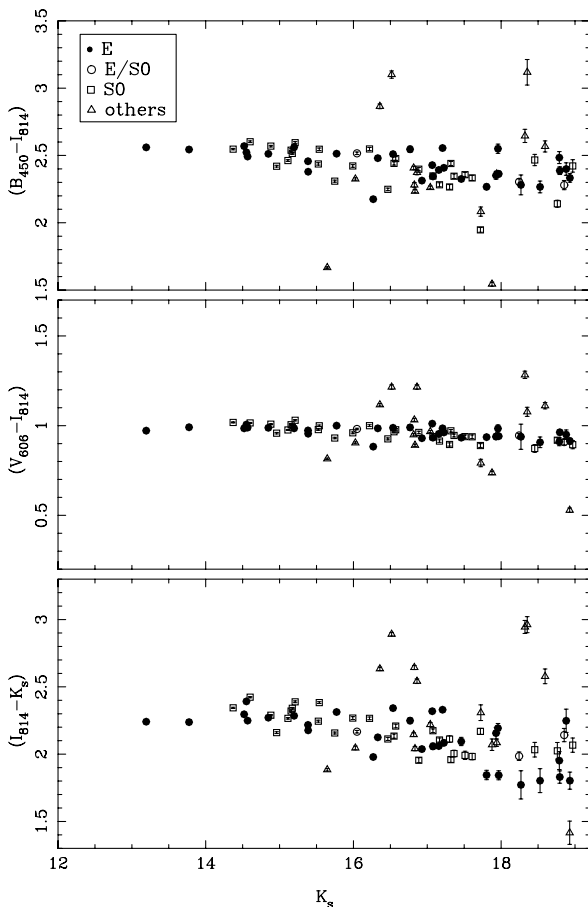


Figure 2. Colour–magnitude diagrams for the $K_s < 19$ sample showing their seeing-matched aperture ($B_{450} - I_{814}$), ($V_{606} - I_{814}$) and ($I_{814} - K_s$) colours as a function of total K_s magnitude. The points are coded on the basis of their optical morphology given in the key. Note the tight sequences exhibited by the colours of the early-type galaxies, especially in ($V_{606} - I_{814}$).

chosen to use visual classifications for our analysis, rather than profile fitting, as all of the claims for morphological evolution of the galaxy populations of distant clusters have used visual estimates of the morphologies (using the same classification scheme as used here, Dressler et al. 1997). Therefore any signatures of this evolution should appear in visually classified samples.

The roll-angle and field centre for the earlier F702W observations were different from the ERO observations analysed here and so there is a slight mismatch in the field coverage between the two data sets. This results in 15 out of the 81 galaxies in our final $K_s < 19$ sample lacking morphologies. Morphological classification of these galaxies was undertaken by one of us (IRS) from the F814W frame. These galaxies are identified by IDs of 4000 and above in Table 1 (galaxies with IDs of 1000 or above fall on the PC chip in the F702W exposure, while ID’s of 2000 and above denote galaxies which had to be demerged interactively in the cataloging process and therefore have close neighbours).

The morphologies of the $K_s < 19$ sample break down as: 31 E, 3 E/S0, 28 S0, 5 Sa and 14 late-type spirals. The core of A 2218 thus exhibits an observed S0-to-E ratio, $N_{S0}/N_E \sim 1$, close to that expected from the evolutionary rate proposed by Dressler et al. (1997), and a large deficit of S0 galaxies compared to the ratio seen in local clusters, $N_{S0}/N_E \sim 2.3$. Within the framework of the S0-transformation model we would expect that roughly half of the S0 population we see in A 2218 had their morphologies transformed since $z \sim 0.5$ (Kodama & Smail 2001).

To determine the representative colours for these galaxies we have chosen to measure photometry from the seeing-matched frames within an aperture that has a radius of three times the half-light radius of the galaxy. The half-light radii, r_{hl} , we quote are simply the radius of a circle containing half the total light of a galaxy on the F814W frame. To estimate the total magnitudes we use the SEXTRACTOR BEST_MAG measurements and correct these to ‘total’ magnitudes using 8.0-arcsec diameter aperture photometry of isolated early-type galaxies on the frame. This correction amounts to -0.05 ± 0.01 mag. A comparison of our half-light radii with the effective radii published by Jørgensen et al. (1999) and Ziegler et al. (2001) from their analyses of the *HST* F702W-band frame shows reasonable agreement, ≤ 20 per cent scatter. The median half-light radius reaches 0.4 arcsec (equivalent to the ground-based seeing) by our limit of $K_s = 19$. For the galaxies with half-light radii below 0.4 arcsec (14 out of the 81) we have chosen to use a fixed aperture of 2.4-arcsec diameter.

To measure the colours of the galaxies we aligned and re-sampled the *HST* frames to the coordinate system defined by the INGRID K_s frame to a tolerance of $\ll 0.1$ arcsec. We then matched the effective PSF on the *HST* and ground-based frames using an iterative Gaussian-convolution technique based on the PSF profiles within the same $3r_{hl}$ radius used in our analysis. For each galaxy we measure the ($B_{450} - I_{814}$), ($V_{606} - I_{814}$) and ($I_{814} - K_s$) colours within the adopted apertures. To judge the sensitivity of our colours to the PSF correction we have reanalysed our frames using PSF convolutions at either extreme of the range of acceptable values and have determined that the ($I_{814} - K_s$) colours, which have the strongest sensitivity to this correction, vary by less than 0.02 mag. We have also remeasured the colours using apertures which are twice as large and determine that the distribution of the early-type population on the colour–colour planes does not significantly alter, with systematic changes in the colours of < 0.02 mag.

We list the aperture photometry for our sample (along with the errors estimated from photon-counting statistics and the variance

of the sky background), our best-estimate of the total K_s mag and the half-light radii in Table 1. Table 1 also gives the positions of the galaxies, this astrometry is tied to the APM coordinate system and has positional accuracy of ≤ 0.5 -arcsec rms. We illustrate the colour–magnitude relations for the galaxies in the different passbands in Fig. 2. The estimated galactic extinction for this field, from Schlegel, Finkbeiner & Davis (1998), is $E(B - V) = 0.024$, giving $E(B_{450} - I_{814}) = 0.058$, $E(V_{606} - I_{814}) = 0.034$, $E(I_{814} - K_s) = 0.038$ and $A_K = 0.01$. We have corrected all colours for extinction but have not corrected the total K_s -band magnitudes. Adopting the Burstein & Heiles (1982) estimate of the extinction reduces the reddening corrections by 25 per cent – or at most 0.01 mag.

2.4 Archival spectroscopy

We expect that field galaxies are likely to comprise a relatively modest fraction of our K_s -selected sample, given the richness and redshift of the cluster we are observing (especially for the early-type galaxies). Nevertheless, we have searched for spectroscopic confirmation of the membership of the galaxies in our sample. The primary sources for this information are Le Borgne, Pelló & Sanahuja (1992), Jørgensen et al. (1999) and Ziegler et al. (2001). We find that a total of 33 of the 81 galaxies in our sample have spectroscopic redshifts. We list the identifications for these galaxies and their redshifts in Table 1, following the naming convention from the NASA/IPAC Extragalactic Database (NED).¹

Of the 33 spectroscopically identified galaxies, only two are non-members, and only one of these (#4010) has an early-type morphology – indicating a field contamination of 3 per cent (for the typically brighter galaxies above the spectroscopic limits). The observed colours of #4010 project it onto the sequence of metal-rich, luminous ellipticals in the cluster. Three other much fainter ellipticals also appear in this region (identified by their large photometric errors in Fig. 4c) and we suggest that these probably represent background field galaxies, although this requires spectroscopic confirmation. The morphological breakdown of the spectroscopic members is: 17/31 Es, 1/3 E/S0s, 13/28 S0s and 2/5 Ss, showing that we have confirmed membership for roughly 40 per cent of the early-type galaxies in our field. In addition, 14 of the early-type galaxies in our sample have high signal-to-noise ratio, moderate resolution spectroscopy, available from Ziegler et al. (2001). We discuss these galaxies in more detail in the next section.

2.5 Stellar population models

We compare the observed colours of the galaxies with the predictions from the GISSEL98 version of the Bruzual & Charlot (1993, 1996) population synthesis code. These use the Padova stellar evolution tracks and the stellar atlas from Lejeune, Buser & Cuisinier (1997), and we adopt a Salpeter (1955) initial mass function (IMF) of ($x = 1.35$) with lower and upper mass cut-offs of 0.1 and $125 M_\odot$. The single stellar population (SSP, a stellar population with a single metallicity, age and IMF) model grids are calculated for six different metallicities ($[M/H] = -2.3, -1.7, -0.7, -0.4, 0.0, \text{ and } +0.4$) and eight ages ($T = 1, 1.5, 2, 3, 5, 7, 10$ and 15 Gyrs). The colours are calculated in the observer’s

frame at the cluster redshift ($z = 0.17$) by redshifting the SSP spectra and convolving these with the filter response functions.

As shown in Fig. 3, the age–metallicity degeneracy can be broken by combining a rest-frame optical colour and a rest-frame optical–infrared colour. This is because the optical–infrared colour [e.g. $(I_{814} - K_s)$] of an old stellar population (>1 Gyr) is primarily determined by the temperature of the red giant branch, which is much more sensitive to the metallicity than the age of the stellar populations (Table 2). In contrast, an optical colour (e.g. $(V_{606} - I_{814})$) is sensitive to *both* age and metallicity in accordance with the predictions of Worthey’s (1994) 2/3 law. Bluer optical colours which sample the rest-frame near-ultraviolet (e.g. $(B_{450} - I_{814})$) at $z = 0.17$) are slightly more sensitive to the metallicity than the 2/3 law suggests, because this colour brackets the rest-frame 4000-Å break, which is sensitive to metal lines (e.g. Fe and Ca HK). Therefore the best combination to break the age–metallicity degeneracy for a cluster at $z \sim 0.2$ is $(V_{606} - I_{814})$ versus $(I_{814} - K_s)$.

3 RESULTS AND DISCUSSION

We show the three colour–magnitude diagrams for our sample in Fig. 2. These illustrate the wide range in luminosity covered in our analysis, nearly 6 mag, with the elliptical and lenticular galaxies evenly spread across this range, except for the brightest two galaxies which are both ellipticals. This figure also shows the relatively homogeneous colours of the majority of the galaxies in our sample. The combined elliptical and lenticular sample exhibits a scatter around their mean relations of 0.11 mag in $(B_{450} - I_{814})$, 0.17 mag in $(I_{814} - K_s)$ and a mere 0.03 mag in $(V_{606} - I_{814})$. However, this scatter is still significantly larger than the mean errors in these colours: $\delta(B_{450} - I_{814}) = 0.02$, $\delta(I_{814} - K_s) = 0.03$ and $\delta(V_{606} - I_{814}) = 0.01$. As we show next, the high precision of our photometry of the early-type galaxies in A 2218 means that we can analyse the small scatter shown in their colours to uncover differences in their stellar populations.

In Fig. 3 we show the two colour–colour diagrams based on the $(B_{450} - I_{814})$ and $(V_{606} - I_{814})$ comparisons with $(I_{814} - K_s)$. We overplot on this figure the grid of models for a range of ages and metallicities (as described in Section 2.5). We indicate in both panels the effects on the observed colours of increasing reddening and redshift (for early-type SEDs). The redshift vector suggests that the bluer end of our sample could suffer field contamination from foreground low-luminosity (but metal-rich) early-type galaxies. This combination of properties is sufficiently rare and the foreground volume is small enough that we do not expect such contamination to be a major problem in our analysis. In general, background galaxies will appear redder in both their optical and optical–infrared colours than the reddest cluster members, and several galaxies with very red colours (and late-type morphologies) are seen: we conclude that these are likely to be background contamination. However, strongly star-forming galaxies at $z \sim 0.7$ can have $(V_{606} - I_{814}) \sim 1$ and $(I_{814} - K_s) \sim 2.2$ – but these should be easily identified from their blue $(B_{450} - I_{814})$ colours (the galaxy #159 appears to be the only possible example of this contamination).

A comparison of the model grids and the observations in Fig. 3 shows good agreement between the regions of the colour–colour plane populated by the observations and those where galaxies are expected to lie on the basis of the stellar population models. However, comparing the ‘orthogonality’ of the age and metallicity

¹The NED is operated by the Jet Propulsion Laboratory, California Institute of Technology, under contract with the National Aeronautics and Space Administration.

Table 1. Galaxy catalogue.

ID	ID _{spec} ^a	α, δ (J2000) 16 ^h , +66°	K_s^{tot}	$(B_{450} - I_{814})$	$(V_{606} - I_{814})$	$(I_{814} - K_s)$	r_{hl} (arcsec)	Morph	z	Note ^b
103	...	35 48.48, 12 1.7	17.72 ± 0.05	2.08 ± 0.03	0.79 ± 0.02	2.31 ± 0.06	1.05	Sdm	...	
129	...	35 46.60, 12 27.0	17.61 ± 0.03	2.33 ± 0.02	0.94 ± 0.01	1.98 ± 0.02	0.41	S0/a	...	
131	L404	35 48.80, 12 9.7	16.93 ± 0.02	2.31 ± 0.01	0.93 ± 0.01	2.04 ± 0.02	0.70	E	0.1708	
137	Z1516	35 46.84, 12 22.9	15.52 ± 0.01	2.44 ± 0.01	0.98 ± 0.00	2.24 ± 0.01	0.77	SB0/a	0.1638	
145	...	35 50.63, 12 1.9	16.82 ± 0.01	2.41 ± 0.01	0.95 ± 0.01	2.15 ± 0.01	0.53	Sab	...	
151	...	35 50.23, 12 5.6	18.24 ± 0.04	2.30 ± 0.02	0.94 ± 0.01	1.99 ± 0.03	0.37	E/S0	...	
153	...	35 52.49, 11 50.6	17.21 ± 0.02	2.55 ± 0.02	0.98 ± 0.01	2.33 ± 0.01	0.28	E	...	
154	B143	35 45.99, 12 32.9	16.54 ± 0.01	2.51 ± 0.01	0.99 ± 0.01	2.34 ± 0.01	0.43	E	0.1659	
159	...	35 45.02, 12 44.7	17.72 ± 0.03	1.95 ± 0.02	0.89 ± 0.01	2.17 ± 0.02	0.36	S0	...	
191	...	35 51.32, 12 7.6	17.30 ± 0.03	2.27 ± 0.02	0.90 ± 0.01	2.11 ± 0.02	0.62	S0	...	
195	...	35 44.97, 12 53.7	17.80 ± 0.05	2.27 ± 0.02	0.94 ± 0.01	1.84 ± 0.04	0.65	E	...	
205	B031	35 56.78, 12 20.5	15.21 ± 0.01	2.60 ± 0.01	1.03 ± 0.00	2.39 ± 0.01	0.75	S0	0.1835	
220	...	35 40.87, 12 36.7	17.08 ± 0.02	2.35 ± 0.01	0.94 ± 0.01	2.17 ± 0.01	0.52	S0	...	
230	...	35 47.60, 12 42.8	15.15 ± 0.01	2.54 ± 0.01	1.00 ± 0.01	2.32 ± 0.01	0.81	S0	...	
232	...	35 46.33, 12 52.0	15.39 ± 0.02	2.38 ± 0.01	0.96 ± 0.00	2.18 ± 0.01	0.80	E	...	
267	...	35 47.41, 13 5.3	17.96 ± 0.06	2.55 ± 0.03	0.98 ± 0.02	2.19 ± 0.03	0.23	E	...	
279	...	35 50.25, 12 19.6	16.47 ± 0.01	2.25 ± 0.01	0.93 ± 0.01	2.11 ± 0.01	0.69	S0	...	
280	B024	35 50.00, 12 23.8	14.37 ± 0.01	2.55 ± 0.01	1.02 ± 0.00	2.34 ± 0.00	1.03	SB0/a	0.1776	Z1552
285	L357	35 51.11, 12 34.1	16.77 ± 0.04	2.55 ± 0.02	0.99 ± 0.02	2.25 ± 0.02	0.32	E	0.1730	
292	L259	35 56.33, 11 51.1	15.11 ± 0.01	2.46 ± 0.01	0.98 ± 0.00	2.27 ± 0.01	0.91	S0	0.1646	
298	B020	35 49.47, 12 36.3	14.96 ± 0.01	2.42 ± 0.01	0.96 ± 0.00	2.16 ± 0.01	0.88	S0	0.1751	Z1580
301	K1	35 49.31, 12 44.7	13.19 ± 0.00	2.56 ± 0.00	0.97 ± 0.00	2.24 ± 0.00	3.50	E	0.1720	cD
303	B117	35 55.92, 12 3.4	16.98 ± 0.02	2.45 ± 0.02	0.98 ± 0.01	2.02 ± 0.02	0.69	E	0.1775	
307	B003	35 56.81, 11 55.5	13.77 ± 0.00	2.54 ± 0.00	0.99 ± 0.00	2.24 ± 0.00	2.84	E	0.1768	Z1437
315	B018	35 51.86, 12 34.3	14.55 ± 0.00	2.52 ± 0.01	1.01 ± 0.00	2.39 ± 0.00	0.71	E	0.1637	Z1662
323	...	35 59.05, 11 47.5	16.82 ± 0.01	2.28 ± 0.02	1.03 ± 0.01	2.64 ± 0.02	0.58	Sc	...	
324	...	35 54.90, 12 18.1	16.83 ± 0.02	2.23 ± 0.01	0.89 ± 0.01	2.04 ± 0.02	0.71	Sab	...	
326	B070	35 53.38, 12 38.6	16.03 ± 0.01	2.32 ± 0.01	0.90 ± 0.01	2.05 ± 0.01	1.16	Sab	0.1791	
333	B048	35 49.05, 13 0.8	15.64 ± 0.01	1.67 ± 0.01	0.82 ± 0.00	1.88 ± 0.01	0.92	Sc	0.1032	
337	B039	35 47.25, 13 16.1	15.20 ± 0.01	2.56 ± 0.01	0.99 ± 0.00	2.28 ± 0.01	0.78	E	0.1800	Z2604
350	...	35 43.50, 12 21.0	18.85 ± 0.08	2.28 ± 0.03	0.91 ± 0.02	2.14 ± 0.05	0.40	E/S0	...	
359	...	35 51.23, 12 55.0	17.23 ± 0.03	2.41 ± 0.02	0.96 ± 0.01	2.08 ± 0.02	0.53	E	...	
368	...	35 59.12, 12 1.3	16.86 ± 0.03	2.37 ± 0.02	1.21 ± 0.01	2.54 ± 0.02	0.70	Sc	...	
376	B064	35 57.43, 12 15.7	15.54 ± 0.01	2.55 ± 0.01	1.00 ± 0.00	2.38 ± 0.01	0.51	S0	0.1820	Z1454
380	...	35 51.06, 13 3.3	18.45 ± 0.10	2.47 ± 0.04	0.87 ± 0.02	2.03 ± 0.05	0.62	S0	...	
387	...	35 56.49, 12 27.1	18.79 ± 0.05	2.39 ± 0.03	0.96 ± 0.01	1.83 ± 0.05	0.27	E	...	
398	...	36 1.26, 11 55.8	17.93 ± 0.06	2.35 ± 0.03	0.94 ± 0.02	2.16 ± 0.04	0.56	E	...	
401	B030	35 59.42, 12 6.6	14.85 ± 0.01	2.51 ± 0.01	0.99 ± 0.00	2.27 ± 0.01	1.29	E	0.1798	Z1466
420	...	35 53.49, 12 57.2	16.52 ± 0.01	3.10 ± 0.03	1.21 ± 0.01	2.89 ± 0.01	0.82	Scd	...	
424	...	36 2.10, 11 58.4	18.93 ± 0.11	2.33 ± 0.03	0.91 ± 0.02	1.80 ± 0.06	0.33	E	...	
428	B028	36 2.33, 11 52.8	14.60 ± 0.00	2.60 ± 0.01	1.01 ± 0.00	2.42 ± 0.00	0.78	S0	0.1830	Z1343
439	...	36 0.57, 12 7.1	16.57 ± 0.02	2.48 ± 0.01	0.98 ± 0.01	2.21 ± 0.01	0.60	S0	...	
449	B087	35 56.72, 12 41.3	16.27 ± 0.01	2.17 ± 0.01	0.88 ± 0.00	1.98 ± 0.01	0.73	E	0.1717	Z1605
457	B121	35 54.67, 13 2.4	18.97 ± 0.10	2.42 ± 0.05	0.89 ± 0.02	2.07 ± 0.05	0.47	S0/a	0.1717	
470	...	35 45.46, 12 8.5	17.16 ± 0.02	2.28 ± 0.01	0.91 ± 0.01	2.11 ± 0.01	0.43	S0	...	
503	B047	35 59.38, 12 53.6	15.38 ± 0.01	2.46 ± 0.01	0.97 ± 0.00	2.22 ± 0.01	0.79	E	0.1747	Z1711
537	Z2660	35 58.39, 13 21.5	16.05 ± 0.01	2.52 ± 0.01	0.98 ± 0.00	2.17 ± 0.01	0.73	E/S0	0.1773	
545	...	36 0.96, 13 10.2	18.76 ± 0.08	2.14 ± 0.03	0.92 ± 0.01	2.02 ± 0.06	0.83	S0	...	
563	B152	35 59.27, 13 33.8	17.16 ± 0.02	2.39 ± 0.01	0.95 ± 0.01	2.06 ± 0.01	0.40	E	0.1787	
571	...	36 0.00, 13 33.5	18.35 ± 0.06	3.12 ± 0.09	1.08 ± 0.03	2.96 ± 0.06	0.87	Scd	...	
599	B159	36 3.81, 13 14.3	17.32 ± 0.02	2.44 ± 0.01	0.97 ± 0.01	1.96 ± 0.02	0.53	S0	0.1731	
612	L143	36 2.64, 13 32.3	16.55 ± 0.02	2.44 ± 0.01	0.97 ± 0.01	2.13 ± 0.02	0.82	S0/a	0.1811	
633	B017	36 4.25, 13 25.3	14.88 ± 0.00	2.57 ± 0.01	1.01 ± 0.00	2.29 ± 0.00	0.70	S0	0.1738	Z2702
634	...	36 4.40, 13 28.7	16.33 ± 0.01	2.48 ± 0.01	0.98 ± 0.01	2.13 ± 0.01	0.64	E	...	
638	...	36 3.81, 13 33.9	15.75 ± 0.01	2.31 ± 0.01	0.93 ± 0.00	2.16 ± 0.01	0.71	S0	...	
646	...	36 2.52, 13 50.8	18.32 ± 0.06	2.64 ± 0.05	1.28 ± 0.02	2.95 ± 0.05	0.56	Sdm	...	
647	...	36 4.75, 13 33.9	17.97 ± 0.03	2.36 ± 0.02	0.94 ± 0.01	1.84 ± 0.03	0.31	E	...	
660	...	35 43.40, 12 28.4	17.94 ± 0.04	2.36 ± 0.02	0.95 ± 0.01	2.09 ± 0.03	0.50	Sb	...	
1018	...	36 0.43, 12 20.8	17.08 ± 0.03	2.34 ± 0.02	0.93 ± 0.01	2.06 ± 0.02	0.83	E	...	
1047	L187	36 0.34, 12 44.2	15.77 ± 0.01	2.51 ± 0.01	1.00 ± 0.00	2.31 ± 0.01	0.46	E	0.1750	
1057	B019	36 2.24, 12 34.5	14.57 ± 0.00	2.49 ± 0.01	0.99 ± 0.00	2.25 ± 0.00	1.27	E	0.1753	
1060	...	36 3.33, 12 32.6	17.36 ± 0.03	2.35 ± 0.02	0.94 ± 0.01	2.00 ± 0.02	0.41	S0	...	
1066	...	36 3.29, 12 36.7	17.51 ± 0.03	2.36 ± 0.02	0.94 ± 0.01	1.99 ± 0.03	0.71	S0	...	
2005	...	35 47.47, 12 24.2	18.53 ± 0.09	2.27 ± 0.04	0.91 ± 0.03	1.80 ± 0.09	0.44	E	...	
2010	...	35 49.18, 12 31.9	18.27 ± 0.13	2.28 ± 0.07	0.94 ± 0.07	1.77 ± 0.10	0.25	E	...	
2011	L389	35 49.32, 12 21.5	17.04 ± 0.04	2.26 ± 0.01	0.97 ± 0.01	2.22 ± 0.01	1.18	Sa	0.1800	
4001	...	36 3.40, 12 3.2	18.93 ± 0.08	1.20 ± 0.02	0.53 ± 0.01	1.42 ± 0.09	0.53	Sd	...	
4002	...	36 4.22, 12 12.0	15.99 ± 0.01	2.42 ± 0.01	0.96 ± 0.01	2.27 ± 0.01	0.92	S0	...	
4003	B185	36 3.54, 12 26.5	17.46 ± 0.03	2.32 ± 0.02	0.93 ± 0.01	2.09 ± 0.03	0.68	E	0.1821	
4004	...	36 6.45, 12 29.3	17.78 ± 0.03	>5.0(2 σ)	3.00 ± 0.18	4.30 ± 0.04	0.29	?	...	

Table 1 – continued

ID	ID _{spec} ^a	α, δ (J2000) 16 ^h , +66 ^o	K_s^{tot}	$(B_{450} - I_{814})$	$(V_{606} - I_{814})$	$(I_{814} - K_s)$	r_{hl} (arcsec)	Morph	z	Note ^b
4005	...	36 6.56, 12 33.1	18.37 ± 0.04	$>4.1(2\sigma)$	1.97 ± 0.17	4.39 ± 0.08	0.36	Sc	...	
4006	...	36 5.97, 12 41.3	18.88 ± 0.08	2.40 ± 0.05	0.95 ± 0.03	2.25 ± 0.09	0.26	E	...	
4007	B036	36 6.41, 12 47.8	15.17 ± 0.01	2.52 ± 0.01	0.99 ± 0.00	2.34 ± 0.01	0.79	SB0	0.1681	
4008	...	36 5.64, 12 49.4	17.88 ± 0.04	1.54 ± 0.02	0.74 ± 0.01	2.07 ± 0.04	0.73	Sb	...	
4009	...	36 7.43, 13 0.3	16.36 ± 0.01	2.86 ± 0.02	1.12 ± 0.01	2.63 ± 0.01	0.73	Sa	...	
4010	B175	36 4.14, 13 2.2	17.07 ± 0.02	2.43 ± 0.02	1.01 ± 0.01	2.32 ± 0.02	0.43	E	0.2913	
4011	...	35 43.63, 13 9.6	18.79 ± 0.08	2.48 ± 0.04	0.91 ± 0.02	1.95 ± 0.07	0.50	E	...	
4012	...	36 6.71, 13 21.7	18.85 ± 0.06	3.73 ± 0.20	1.81 ± 0.05	3.69 ± 0.06	0.19	?	...	
4013	B015	35 44.12, 13 20.4	14.52 ± 0.00	2.57 ± 0.01	0.98 ± 0.00	2.30 ± 0.00	0.96	E	0.1778	
4014	Z2738	36 4.85, 13 42.5	16.22 ± 0.01	2.55 ± 0.01	1.00 ± 0.01	2.27 ± 0.01	0.46	S0	0.1742	
4015	...	36 9.28, 13 47.6	18.59 ± 0.04	2.57 ± 0.04	1.11 ± 0.02	2.58 ± 0.05	0.28	Sc	...	

^aZ: Ziegler et al. (2001), B: Butcher et al. (1983), L: Le Borgne et al. (1992), K: Kristian et al. (1978).

^bZiegler et al. (2001).

?Unclassifiable morphology.

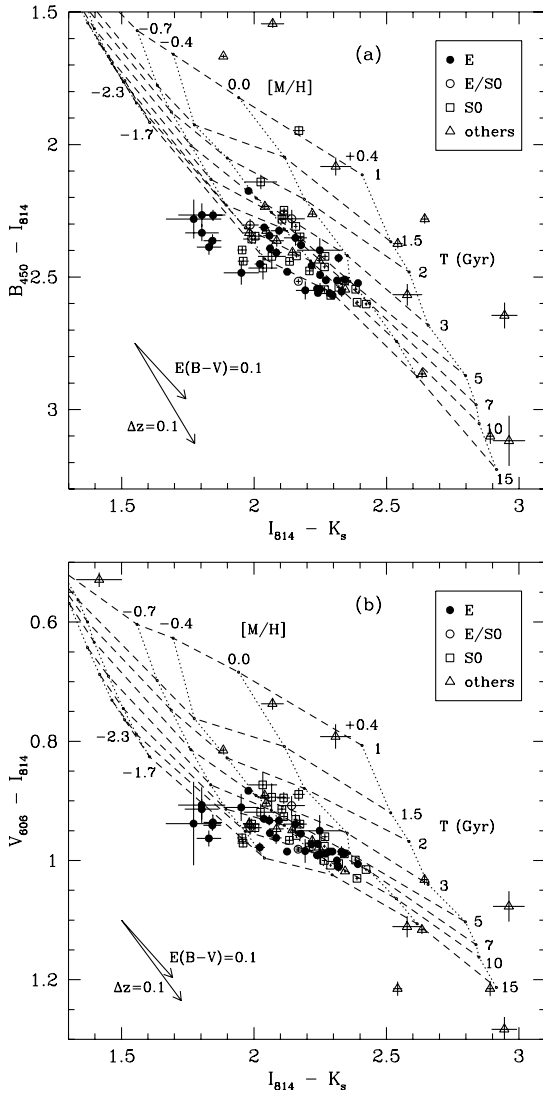


Figure 3. Colour–colour diagrams for the $K_s < 19$ sample comparing the $(B_{450} - I_{814})$ and $(V_{606} - I_{814})$ versus $(I_{814} - K_s)$ planes. The points are coded on the basis of their optical morphology as given in the key. The two vectors show the effects on the galaxy colours of increasing the internal reddening and increasing redshift (assuming an early-type spectral energy distribution).

tracks on the two colour–colour planes in Fig. 3 we can see that the $(V_{606} - I_{814})$ grid provides a better differentiation between age and metallicity than $(B_{450} - I_{814})$, as is expected from the discussion in Section 2.5. Hence, for the remainder of our analysis we will concentrate on the $(V_{606} - I_{814}) - (I_{814} - K_s)$ colour–colour plane and compare the detailed distribution of the galaxies on it to the model tracks.

The dominant feature in the $(V_{606} - I_{814})$ panel in Fig. 3 [and also shown by the $(B_{450} - I_{814})$ plot] is a tight locus of points in the region of the grid corresponding to the oldest and most metal rich stellar populations. These galaxies are typically the brightest early-type galaxies in the cluster (Fig. 2). Their locus traces what appears to be a metallicity sequence – spanning a range of ~ 0.5 dex in $[M/H]$ – at a single age (~ 7 Gyr – although the uncertainty in the metallicities and the relative calibration of the colours and grids means that the reader should view the ages as defined on a relative, rather than an absolute scale). This can be seen more clearly in Fig. 4, which illustrates the $(V_{606} - I_{814}) - (I_{814} - K_s)$ distributions for the morphologically classified elliptical and lenticular galaxies (we place the three E/S0 galaxies into the latter sample). The fainter galaxies (identified by the larger photometric errors) extend this sequence to lower $[M/H]$, but also appear to show a wider spread in ages.

Looking more closely at Fig. 3, we see that a number of the faintest elliptical galaxies fall just outside the region covered by the model predictions. This effect is strongest in the $(B_{450} - I_{814})$ plot, whereas in the $(V_{606} - I_{814})$ plot (which we concentrate on), five of the six discrepant points lie within 1σ of the grid and the sixth is less than 2σ away. Unfortunately, none of these galaxies have spectroscopic information to confirm their cluster membership. Assuming they are cluster members, it is likely that this discrepancy reflects inherent uncertainties in the model grid as a result of the lack of good libraries of old, sub-solar metallicity stars that are needed to reliably model this region of the grid (see Charlot, Worthey & Bressan 1996). These uncertainties may effect both the absolute and relative ages derived from the model grids in this region and in the following we have tried to reflect this uncertainty when discussing the conclusions we draw.

To test the reliability of our analysis we compare our results for the 14 galaxies in common with the spectroscopic sample of Ziegler et al. (2001). We note that these galaxies are typically the brighter ones in our sample, with a median magnitude of $K_s = 15.1$, the faintest having $K_s = 16.3$ ($0.2L_{K_s}^*$). We find that most of the galaxies are consistent in both analyses with a single age

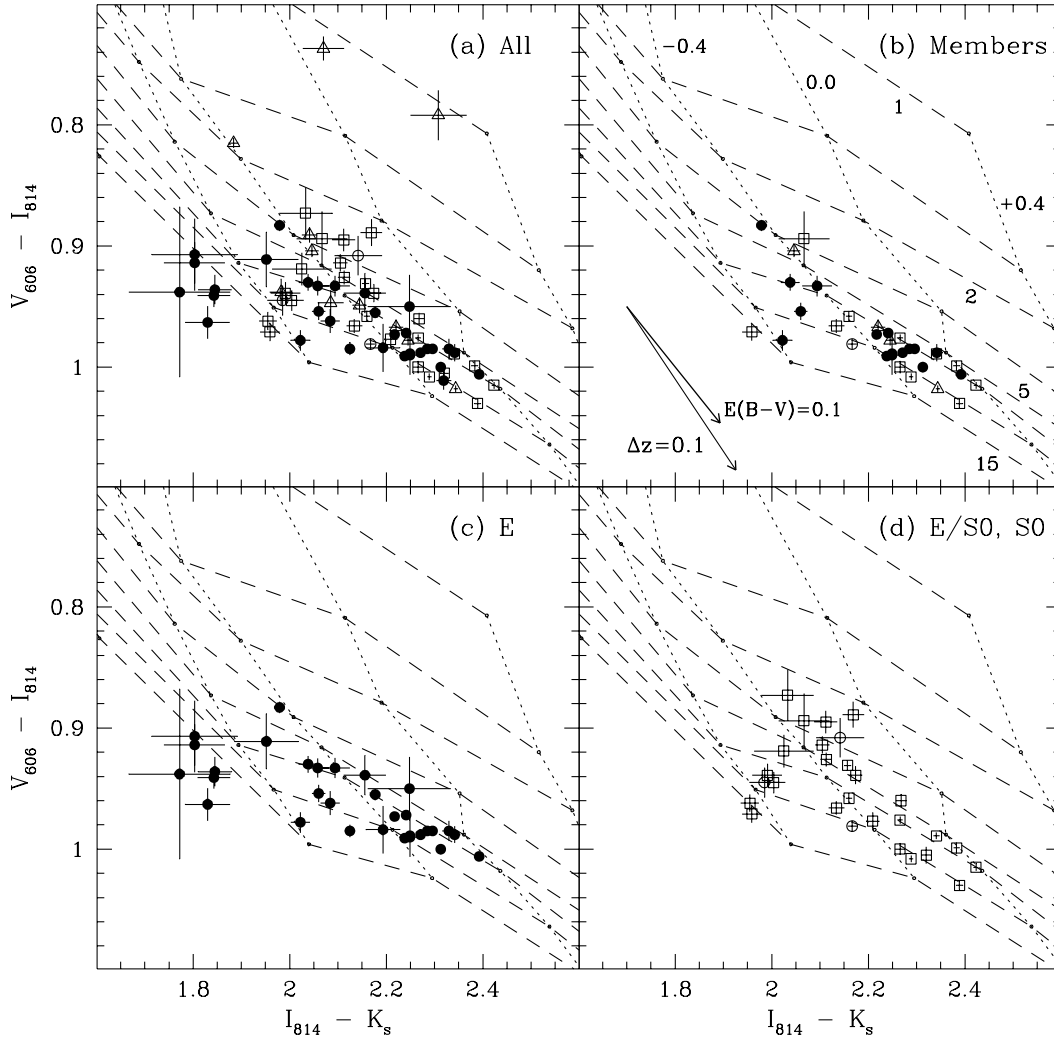


Figure 4. A mosaic of colour–colour plots illustrating their distribution in the $(V_{606} - I_{814}) - (I_{814} - K_s)$ plane for the $K_s < 19$ sample. The points are coded on the basis of their optical morphology using the same symbols as Fig. 3. The four panels show: (a) the whole sample, (b) just the spectroscopically-confirmed members, (c) only the morphologically-typed ellipticals and (d) only the morphologically classified S0s and E/S0. The relative luminosities of the various galaxies can be gauged from the size of the error bars on the data points.

Table 2. The sensitivity to age and metallicity of the colours used in our analysis. The rate of change of colour is determined for $2 < T(\text{Gyr}) < 10$ and $-0.7 < [M/H] < 0.0$. The ratio, $[d(\text{col})/d[M/H]]/[d(\text{col})/d \log T]$, is also shown in the final column.

Colour	$d(\text{col})/d[M/H]$	$d(\text{col})/d \log T$	Ratio
$(B_{450} - I_{814})$	0.53	0.56	0.96
$(V_{606} - I_{814})$	0.15	0.22	0.67
$(I_{814} - K_s)$	0.76	0.45	1.73

(~ 7 – 8 Gyr) and a range of metallicity. However, one galaxy stands out in our sample – #449, the bluest confirmed elliptical member in Fig. 4b – the luminosity-weighted age we derive for the stellar population in this galaxy is a mere 3 Gyr (suggesting that the stellar population which currently dominates the galaxy’s luminosity was formed at a redshift of only $z \lesssim 0.5$). This galaxy also stands out in the analysis of Ziegler et al. as the youngest galaxy by far in the joint sample, with an estimated age of around ~ 1.5 Gyr. This comparison with the results of the more traditional

spectroscopic approach clearly supports the reliability of the optical/near-infrared photometric technique for analysing the stellar populations of early-type galaxies in distant clusters. Moreover, the photometric method requires only a fraction of the time needed for spectroscopic surveys and can probe into fainter luminosities.

Turning back to Fig. 4 we now compare the colours of the different morphological subsamples. The sequence defined by the redder and more luminous galaxies appears in both the E and S0+E/S0 subsamples, as well as in the spectroscopically confirmed members. There maybe a slight tendency for the bright S0+E/S0 sample to show a wider age spread than the Es [$\sigma_T(\text{S0}) = 2.2$ Gyr versus $\sigma_T(\text{E}) = 0.8$ Gyr at $K_s < 16.0$]. The likelihood that this difference in dispersions arises by chance from the joint sample is only slight, ≤ 0.1 per cent. However, this comparison is very sensitive to the exact magnitude limit used.

Nevertheless, there is an even more striking difference between the two morphological subsamples at the lowest luminosities. To emphasize the variation in the properties of the lowest luminosity galaxies, we show the colour–colour plot for the fainter ($K_s > 17$, $\lesssim 0.1L_{\text{K}}$) early-type galaxies in Fig. 5. Here, while the faint

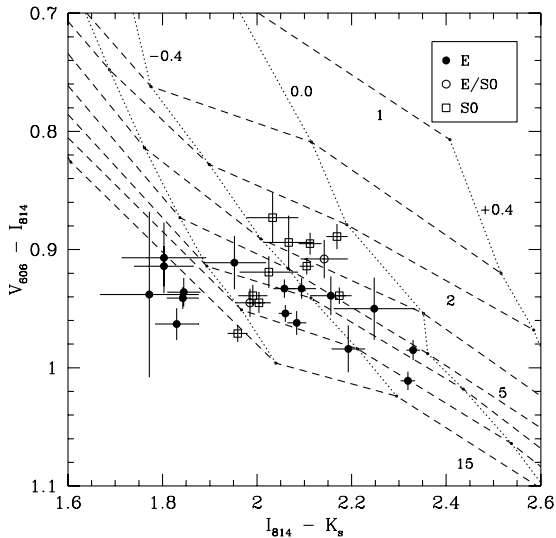


Figure 5. This plot compares the distribution of the faintest early-type galaxies ($K_s > 17$) in our sample with the predictions of the stellar population models. The striking difference in the distribution of faint E and S0 galaxies is obvious.

ellipticals appear to extend the metallicity sequence defined by the brighter ellipticals (and S0’s), the fainter S0 galaxies show an almost orthogonal colour–colour relationship to that exhibited by the faint ellipticals and all the more luminous galaxies [qualitatively similar behaviour is seen in the equivalent ($B_{450} - I_{814}$) plot]. This reversal in the colour trends results from the appearance of a population of faint S0 with relatively blue ($V_{606} - I_{814}$) colours, indicating luminosity-weighted mean ages of only 2–5 Gyr and metallicities of $[M/H] \sim -0.2$ for the stellar populations in these galaxies. It is unlikely that all of the stars in these galaxies were formed in the most recent star formation event and hence the luminosity-weighted ages are in fact upper limits on the epoch of the most recent star formation.

To quantify the prevalence of this population, we arbitrarily define ‘young’ as a luminosity-weighted age of < 5 Gyr and find that half of the $K_s > 17$ S0 galaxies are young (or 30 per cent of the whole S0 population, Fig. 6), in contrast none of the faint E’s fall in this category. This is a high enough proportion of the S0 population (given the duration of the ‘young’ phase) to suggest that most of the faint lenticular galaxies in the cluster must have passed through this phase. To quantify the extent of any possible luminosity bias in our analysis, we determine that the fading of the stellar populations of the young S0 galaxies by the present-day should not exceed 0.2 mag in K_s , compared to the more luminous, evolved galaxies in the cluster (Smail et al. 1998; Kodama & Bower 2001). Taking this modest luminosity bias into account we find that it would reduce the proportion of ‘young’ S0s in an unbiased sample by only 5 per cent.

The behaviour exhibited by the faint lenticular population is very similar to that seen in the ‘UV+’ galaxies identified in a photometric survey of X-ray luminous clusters at $z \sim 0.2$ by Smail et al. (1998). Their relatively shallow ground-based imaging lacked the precision necessary for an analysis of the type undertaken here. Nevertheless, they used the increased sensitivity to differences in the stellar populations available from their ($U - B$) colours to identify a class of ultraviolet (UV)-bright galaxies which showed strong 4000 \AA breaks (‘UV+’) indicative of evolved stellar populations. They suggested that these UV+

galaxies represented the fading progenitors of the cluster S0 population. The UV+ class constitutes approximately 50 per cent of the faint cluster population ($< 0.2L_{\text{UV}}^*$) which exhibit strong 4000 \AA breaks. Based on the *HST* imaging of a handful of the UV+ galaxies in the core of A 2390, Smail et al. (1998) suggest that the majority of these galaxies have S0 morphologies. The luminosities, colours and morphologies of the UV+ population are thus similar to the faint, blue S0 population identified here. Interestingly, Smail et al. (1998) found that the radial profile of the UV+ population is indistinguishable from that of the luminous, evolved galaxies in these clusters, suggesting that these galaxies are not recent additions to the cluster population.

Finally we discuss the characteristics of the S0 population in the context of the morphological evolution discussed by Dressler et al. (1997) and Poggianti et al. (1999). The evolution in the number of S0 galaxies in clusters at $z > 0.3$ – 0.6 observed by Dressler et al. (1997) suggests that roughly two-thirds of the S0 population in a $z = 0.17$ cluster would have transformed their morphologies in the last 3 Gyr (since $z \sim 0.5$), with half of these occurring in the last 1–2 Gyr. Adopting a 1–2 Gyr delay between the termination of star formation and the morphological transformation occurring, as is needed to explain the lack of blue S0 galaxies in the distant clusters and the large number of passive galaxies with late-type morphologies (Poggianti et al. 1999; Kodama & Smail 2001), then we would expect that 60–70 per cent of the S0 galaxies in A 2218 were forming stars 4–5 Gyr prior to $z = 0.17$, and 30 per cent of them within the last 2–3 Gyr.

To estimate the luminosity-weighted ages for the composite stellar populations in these galaxies at a later time we need to assume a model for their previous star formation. If we assume that these progenitors were forming stars at a constant rate (or slightly declining) since their formation at high redshift, as normal early- and mid-type spiral galaxies are believed to do, then for the 30 per cent of the S0 population which is predicted to have had terminated its star formation in the 2–3 Gyr before $z = 0.17$ (equivalent to $z \sim 0.5$ in the cosmology we adopt) they would have luminosity-weighted ages of $\lesssim 5$ Gyr when seen at $z = 0.17$. This model is thus consistent with the 30 per cent fraction of the S0 population which we observe to have luminosity-weighted ages of $\lesssim 5$ Gyr. Indeed, the smooth growth of the S0 fraction in the clusters reported by Dressler et al. (1997) is also mirrored by the nearly flat distribution of estimated ages for this population, seen in Fig. 6. Therefore, our observations support a scenario where the fraction of S0s in the clusters is smoothly increasing towards the present-day as a result of a slow morphological and spectroscopic transformation of star forming spiral galaxies into passive, S0 cluster members.

4 CONCLUSIONS

(1) We present precise optical and near-infrared photometry of a sample of 81 galaxies in the core regions of the rich cluster A 2218 at $z = 0.17$ (a look-back time of 3 Gyr).

(2) We compare the optical and optical–infrared colours of the morphologically classified early-type galaxies in our sample with the predictions of stellar population models, spanning a range in metallicity and age. The models show good agreement in the regions of the colour–colour plane which are populated by the observational data.

(3) By comparing our results with those from a recent spectroscopic survey of the stellar populations in galaxies in A 2218, we confirm the reliability of the photometric analysis

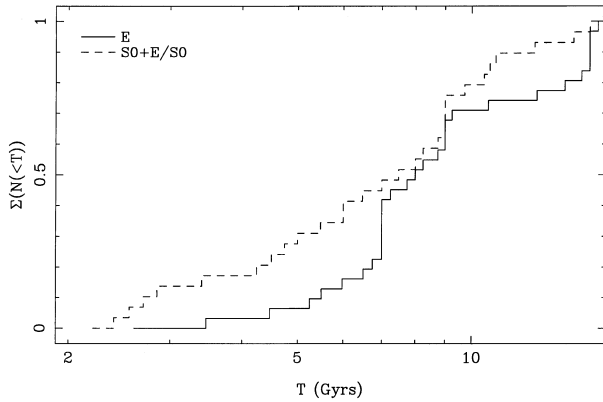


Figure 6. The cumulative distributions of the estimated luminosity-weighted relative ages of the full elliptical and lenticular samples. Note the relatively flat distribution of derived ages for the S0+E/S0 sample, compared with the more uniform and older ages seen in the ellipticals, where the mean stellar populations in 80 per cent of the galaxies are older than ~ 7 Gyr. We stress that these estimated ages should be viewed as relative rather than absolute values.

technique. We show that both techniques identify galaxies with relatively young stellar populations.

(4) The colours of the more luminous early-type galaxies ($\geq L_K^*$) in the cluster are well described by a sequence of varying metallicity for the stellar population at a constant age. This is in agreement with the results of the analysis of the spectral line strengths in similar luminosity galaxies in A 2218 (Ziegler et al. 2001) and results from the spectroscopic and photometric analysis of galaxies in higher-redshift clusters (Kodama & Arimoto 1997; Jones et al. 2000).

(5) In contrast the faintest early-type galaxies ($\leq 0.1L_K^*$) show a large spread in their optical and optical–infrared colours. Around 30 per cent of the S0 galaxies in A 2218 (and half of the fainter examples) exhibit mean luminosity-weighted ages for their stellar populations of ≤ 5 Gyr. This suggests that these galaxies were actively forming stars at $z \leq 0.5$. The proportion of these ‘young’ S0 galaxies is consistent with the rate of evolution of the S0 fraction in distant clusters reported by Dressler et al. (1997). Further support for the gradual growth of the S0 population comes from the relatively flat age-distribution we derive for these galaxies. In contrast, the vast majority of the morphologically classified elliptical galaxies across all luminosities show evolved stellar populations.

(6) Most of the galaxies we see which show signs of recent activity lie below the magnitude limits reached by spectroscopic studies of galaxies in distant clusters. This highlights the urgent need to exploit the increased sensitivity available with 8-m telescopes to measure detailed line indices in low-luminosity members of intermediate and moderate redshift clusters.

(7) We have demonstrated the power of photometric analysis of the optical–infrared colours of early-type cluster galaxies to uncover information about their star formation histories. This type of precision photometric analysis should be extended to more distant clusters (in which it is predicted that a higher fraction of the S0 galaxies should show signs of past star formation activity) and to wider fields at intermediate redshifts to search for the signatures of the physical processes responsible for the spectroscopic and morphological transformations at the heart of the formation of S0 galaxies.

ACKNOWLEDGMENTS

This paper is based upon observations obtained with the NASA/ESA *Hubble Space Telescope* which is operated by STScI for the Association of Universities for Research in Astronomy, Inc., under NASA contract NAS5-26555 and on observations made with the William Herschel Telescope operated on the island of La Palma by the Isaac Newton Group in the Spanish Observatorio del Roque de los Muchachos of the Instituto de Astrofísica de Canarias.

We thank Warrick Couch, Roger Davies, Bianca Poggianti, Ray Sharples, Alex Vazdekis and Bodo Ziegler for useful conversations and help. We especially thank the referee, Alfonso Aragón-Salamanca, for his helpful and constructive comments which improved the content and presentation of the paper. IRS acknowledges support from the Royal Society. HK and GPS acknowledge support from PPARC. TK acknowledges support through a Research Fellowship for Young Scientists from the Japan Society for the Promotion of Science.

REFERENCES

- Aaronson M., 1978, *ApJ*, 221, L103
 Andreon S., 1998, *ApJ*, 501, 533
 Aragón-Salamanca A., Ellis R. S., Couch W. J., Carter D., 1993, *MNRAS*, 262, 764
 Bertin E., Arnouts S., 1996, *A&AS*, 117, 393
 Bruzual G. A., Charlot S., 1993, *ApJ*, 405, 538
 Bruzual G. A., Charlot S., 1996, *GISSEL96 Manual* (version 1996.1)
 Burstein D., Heiles C., 1982, *AJ*, 87, 1165
 Butcher H., Wells D. C., Oemler A., 1983, *ApJS*, 52, 183
 Charlot S., Worthey G., Bressan A., 1996, *ApJ*, 457, 625
 Cole S. M. et al., 2001, *MNRAS*, submitted
 van Dokkum P. G., Franx M., Kelson D. D., Illingworth G. D., Fisher D., Fabricant D., 1998, *ApJ*, 500, 714
 Dressler A., Oemler A., Couch W. J., Smail I., Ellis R. S., Barger A., Butcher H., Poggianti B. M., Sharples R. M., 1997, *ApJ*, 490, 577
 Ellis R. S., Smail I., Dressler A., Couch W. J., Oemler A., Butcher H., Sharples R. M., 1997, *ApJ*, 483, 582
 Fabricant D., Franx M., van Dokkum P., 2000, *ApJ*, 539, 577
 Fasano G., Poggianti B. M., Couch W. J., Bettoni D., Kjaergaard P., Moles M., 2000, *ApJ*, 542, 673
 Fruchter A. S., Hook R. N., 1997, in Tescher A., eds, *Applications of Digital Image Processing*, Proc. SPIE, 3164, 120
 Holtzman J. A., Burrows C. J., Casterno S., Hester J. J., Trauger J. T., Watson A. M., Worthey G., 1995, *PASP*, 107, 1065
 Jones L. A., Smail I., Couch W. J., 2000, *ApJ*, 528, 118
 Jørgensen I., 1999, *MNRAS*, 306, 607
 Jørgensen I., Franx M., Hjorth J., van Dokkum P. G., 1999, *MNRAS*, 308, 833
 Kelson D. D., van Dokkum P. G., Franx M., Illingworth G. D., Fabricant D., 1997, *ApJ*, 478, 13
 Kelson D. D., Illingworth G. D., van Dokkum P. G., Franx M., 2000, *ApJ*, 531, 184
 Kristian J., Sandage A., Westphal J. A., 1978, *ApJ*, 221, 383
 Kneib J.-P., Ellis R. S., Smail I., Couch W. J., Sharples R. M., 1996, *ApJ*, 471, 643
 Kodama T., Arimoto N., 1997, *A&A*, 320, 41
 Kodama T., Arimoto N., Barger A., Aragón-Salamanca A., 1998, *A&A*, 334, 99
 Kodama T., Bower R. G., 2001, *MNRAS*, submitted
 Kodama T., Smail I., 2001, *MNRAS*, submitted
 Kuntschner H., 2000, *MNRAS*, 315, 184
 Le Borgne F. J., Pelló R., Sanahuja B., 1992, *A&AS*, 95, 87
 Lejeune Th., Cuisinier F., Buser R., 1997, *A&AS*, 125, 229
 Moore B., Lake G., Katz N., 1998, *ApJ*, 495, 139

- Peletier R., Balcells M., 1996, *AJ*, 111, 2238
- Persson S. E., Murphy D. C., Kreminski W., Roth M., Rieke M. J., 1998, *AJ*, 116, 2475
- Poggianti B. M., Smail I., Dressler A., Couch W. J., Barger A. J., Butcher H., Ellis R. S., Oemler A., 1999, *ApJ*, 518, 576
- Salpeter E. E., 1955, *ApJ*, 121, 161
- Schlegel D., Finkbeiner D. P., Davis M., 1998, *ApJ*, 500, 525
- Smail I., Dressler A., Couch W. J., Ellis R. S., Oemler A., Butcher H., Sharples R. M., 1997, *ApJS*, 110, 213
- Smail I., Edge A. C., Ellis R. S., Blandford R. D., 1998, *MNRAS*, 293, 124
- Vazdekis A., Arimoto N., 1999, *ApJ*, 525, 144
- Vazdekis A., Peletier R. F., Beckman J. E., Casuso E., 1997, *ApJS*, 111, 203
- Worthey G., 1994, *ApJS*, 95, 107
- Ziegler B., Bower R. G., Smail I., Davies R. L., Lee D., 2001, *MNRAS*, submitted

This paper has been typeset from a \TeX/L\TeX file prepared by the author.